Ohira et al. Progress in Earth and Planetary Science (2016) 3:18
DOI 10.1186/s40645-016-0097-2

Progress in Earth and Planetary Science

RESEARCH ARTICLE Open Access

Ultrahigh-pressure acoustic wave velocities of SiO_2-Al_2O_3 glasses up to 200 GPa

Itaru Ohira[1*], Motohiko Murakami[1], Shinji Kohara[2,3], Koji Ohara[2] and Eiji Ohtani[1,4]

Abstract

Extensive experimental studies on the structure and density of silicate glasses as laboratory analogs of natural silicate melts have attempted to address the nature of dense silicate melts that may be present at the base of the mantle. Previous ultrahigh-pressure experiments, however, have been performed on simple systems such as SiO_2 or $MgSiO_3$, and experiments in more complex system have been conducted under relatively low-pressure conditions below 60 GPa. The effect of other metal cations on structural changes that occur in dense silicate glasses under ultrahigh pressures has been poorly understood. Here, we used a Brillouin scattering spectroscopic method up to pressures of 196.9 GPa to conduct in situ high-pressure acoustic wave velocity measurements of SiO_2-Al_2O_3 glasses in order to understand the effect of Al_2O_3 on pressure-induced structural changes in the glasses as analogs of aluminosilicate melts. From 10 to 40 GPa, the transverse acoustic wave velocity (V_S) of Al_2O_3-rich glass (SiO_2 + 20.5 mol% Al_2O_3) was greater than that of Al_2O_3-poor glass (SiO_2 + 3.9 mol% Al_2O_3). This result suggests that SiO_2-Al_2O_3 glasses with higher proportions of Al ions with large oxygen coordination numbers (5 and 6) become elastically stiffer up to 40 GPa, depending on the Al_2O_3 content, but then soften above 40 GPa. At pressures from 40 to ~100 GPa, the increase in V_S with increasing pressure became less steep than below 40 GPa. Above ~100 GPa, there were abrupt increases in the P-V_S gradients (dV_S/dP) at 130 GPa in Al_2O_3-poor glass and at 116 GPa in Al_2O_3-rich glass. These changes resemble previous experimental results on SiO_2 glass and $MgSiO_3$ glass. Given that changes of dV_S/dP have commonly been related to changes in the Si-O coordination states in the glasses, our results, therefore, may indicate a drastic structural transformation in SiO_2-Al_2O_3 glasses above 116 GPa, possibly associated with an average Si-O coordination number change to higher than 6. Compared to previous acoustic wave velocity data on SiO_2 and $MgSiO_3$ glasses, Al_2O_3 appears to promote a lowering of the pressure at which the abrupt increase of dV_S/dP is observed. This suggests that the Al_2O_3 in silicate melts may help to stabilize those melts gravitationally in the lower mantle.

Keywords: Glass structure, Brillouin scattering, High pressure, Acoustic wave velocity, Heterogeneity of Earth's core-mantle boundary

Background

There are regions at the base of the mantle where anomalous reductions of seismic wave velocities occur (e.g., Garnero and Helmberger 1995; Mori and Helmberger 1995). These are known as ultralow velocity zones (ULVZs). They vary in thickness from 5 to 40 km just above the core-mantle boundary (CMB) where there is a ~10–30 % seismic velocity reduction (e.g., Garnero et al. 1998). The possible presence of silicate melts resulting from partial melting of the lowermost mantle minerals (e.g., Williams and Garnero 1996) or remnants of the dense basal magma ocean (Labrosse et al. 2007) has been proposed to explain these anomalous seismic reductions at the CMB. Silicate melts under lower mantle conditions are not well understood because of the technical difficulties involved in conducting experiments on silicate melts under relevant high-pressure conditions. Although very recent in situ synchrotron X-ray diffraction measurements of basaltic melt were successful under lower mantle pressures (Sanloup et al. 2013), the pressure conditions of the measurements were limited to below ~60 GPa.

* Correspondence: i.ohira@dc.tohoku.ac.jp
[1]Department of Earth Science, Graduate School of Science, Tohoku University, Sendai 980-8578, Japan
Full list of author information is available at the end of the article

Silicate glasses have been used as possible analogs for silicate melts to understand the nature of dense magmas in the lower mantle (e.g., Murakami and Bass 2010, 2011; Petitgirard et al. 2015). Although the structural changes that silicate glasses undergo cannot be assumed to be a completely valid model for silicate melts, previous experimental works have shown that the Si-O coordination numbers of SiO_2 glass and a molten basalt appear to change in generally similar ways (Meade et al. 1992; Lin et al. 2007; Sato and Funamori 2008, 2010; Benmore et al. 2010; Zeidler et al. 2014; Sanloup et al. 2013). This suggests that the analogy of the structural change that silicate glasses undergo to the changes in silicate melts appears to work well for Si-O coordination number and probably for most structural aspects at least above 10 GPa (Sanloup et al. 2013).

The behavior of silicate glasses under ultrahigh pressures above 100 GPa has recently been explored by acoustic wave velocity measurements using in situ high-pressure Brillouin scattering spectroscopy as a way to monitor structural changes in silicate melts under ultrahigh-pressure conditions (Murakami and Bass 2010, 2011). The results for SiO_2 glass (Murakami and Bass 2010) showed that the changes in acoustic wave velocity occur at the same pressure as the changes in the Si-O coordination number of SiO_2 glass from 4 to 6, inferred from in situ synchrotron X-ray diffraction measurements up to 100 GPa (Sato and Funamori 2010). This indicates that acoustic wave velocity can be a good indicator for tracking the pressure evolution of the Si-O coordination number of silicate glasses. Murakami and Bass (2010) also reported an abrupt increase of P-V_S gradient (dV_S/dP) in SiO_2 glass above ~140 GPa, which was also observed in $MgSiO_3$ glass at ~133 GPa (Murakami and Bass 2011) and proposed the possibility of a further structural change such as a gradual increase of the average Si-O coordination number from 6 to 6^+. Such a structural change may increase the densities of silicate melts significantly, and therefore can constrain the dynamics of silicate melts that may exist at the base of the mantle.

Acoustic wave velocity measurements of silicate glasses under ultrahigh-pressure conditions have so far been conducted only in very simple systems such as SiO_2 and $MgSiO_3$ (Murakami and Bass 2010, 2011), and it is still unclear whether the densification mechanisms inferred from the velocity measurements of SiO_2 or $MgSiO_3$ glasses are directly applicable to the silicate glasses/melts in more realistic compositional systems in nature. To address this issue, we focus on the effect of Al_2O_3, the second-most abundant oxide in natural magma, on structural changes in silicate glasses. The SiO_2-Al_2O_3 system is the simplest from among the aluminous silicate systems. A number of previous studies have reported structural features at ambient pressure, as inferred by Raman scattering (Kato 1976; McMillan and Piriou 1982), infrared absorption (Poe et al. 1992a; Okuno et al. 2005), X-ray diffraction (Morikawa et al. 1982; Okuno et al. 2005), nuclear magnetic resonance (NMR) spectroscopic techniques (Risbud et al. 1987; Sato et al. 1991; Poe et al. 1992a, b; Sen and Youngman 2004; Weber et al. 2008), and by molecular dynamics (MD) computer simulations (Poe et al. 1992a, b; Linh and Hoang 2007).

Previous high-pressure experiments using NMR spectroscopic techniques showed that the proportion of five- and sixfold coordination of Al in aluminosilicate glasses quenched from high pressures and temperatures corresponding to the upper mantle is positively correlated with pressure (e.g., Yarger et al. 1995; Lee et al. 2004; Allwardt et al. 2005, 2007), suggesting that the increase in Al-O coordination number occurs at lower pressures than that in Si-O. In situ XRD measurement for $CaAl_2Si_2O_8$ glass supports the conclusions inferred from those NMR studies (Drewitt et al. 2015). However, the role Al_2O_3 plays in the structure and physical properties of silicate glasses and melts under lower mantle pressures is still unknown.

To advance our understanding on the effect the presence of Al_2O_3 has on the structures of aluminosilicate glasses at lower mantle pressures, we performed in situ high-pressure Brillouin scattering measurements of SiO_2-Al_2O_3 glasses up to pressures of 196.9 GPa. Based on the results, we discuss the effect of Al_2O_3 on the densification mechanism of aluminosilicate glasses at the lowermost mantle pressure conditions and consider possible implications for the dynamics of dense silicate melts at the base of the mantle.

Methods

Two aluminosilicate glass samples, $SiO_2 + 3.9$ mol% Al_2O_3 glass (SA1) and $SiO_2 + 20.5$ mol% Al_2O_3 glass (SA2) were synthesized by means of a containerless levitation heating method at the SPring-8 BL04B2 beamline at the SPring-8 synchrotron radiation facility in Hyogo, Japan (Kohara et al. 2007). By using this method, both contamination of the molten samples and heterogeneous nucleation by crucible surfaces were avoided. Blocks of silicate powders weighing 1–2 mg were levitated in air using an aerodynamic levitator and heated by a 100 W CO_2 laser beam. After melting the samples, small, rapidly cooled vitreous spheroids (~0.5–1 mm in diameter) were obtained by blocking the CO_2 laser.

The X-ray diffraction data for the SA1 and SA2 were corrected for polarization, absorption, and background, and the contribution of Compton scattering was subtracted using standard analysis procedures (see Kohara et al. 2007 for the technical details). The corrected data sets were normalized to give the Faber-Ziman total

structure factor $S(Q)$. The radial distribution function RDF(r) was obtained by a Fourier transformation of $S(Q)$ (Fig. 1). The composition and homogeneity of those glasses were confirmed by scanning electron microscope with energy-dispersive X-ray spectrometer (SEM-EDS). The compositional errors in the Al_2O_3 mol% were ±0.4 % in SA1 and ±0.5 % in SA2, estimated from the standard deviation of 10 analyzed points in SA1 and SA2.

In situ high-pressure acoustic wave velocity measurements were carried out at room temperature using a high-pressure Brillouin scattering spectroscopic system combined with a symmetric-type diamond anvil cell apparatus at Tohoku University (see also Mashino et al. 2016). The acoustic wave velocities, i.e., a longitudinal wave velocity (V_P) and a transverse wave velocity (V_S), in a symmetric geometry are calculated from the relation (Whitfield et al. 1976):

$$V = \frac{\Delta\omega\lambda}{2\sin(\theta/2)}$$

where λ is the laser wavelength of the incident laser beam and θ is the external scattering angle. $\Delta\omega$ indicates the Brillouin frequency shifts of longitudinal or transverse acoustic modes. An argon ion laser with a wavelength of 532 nm was used as the probe beam. The incident laser beam was focused to a spot size of ~20 μm. The scattered light was analyzed by a six-pass tandem Fabry-Pérot interferometer. In all Brillouin experiments, we used a symmetric scattering geometry with a 50° external scattering angle. A borosilicate crown optical glass (BK7) was used to calibrate the symmetric scattering geometry.

The SiO_2-Al_2O_3 glass powders were loaded without a pressure-transmitting medium into a 50 or 70 μm hole drilled in a rhenium gasket. The samples were compressed with 100 and 130 μm beveled diamond anvils and a 300 μm non-beveled diamond anvil. Pressure was determined using the Raman T_{2g} mode of the diamond anvil (Akahama and Kawamura 2004) by measuring 3–5 points at the center of the incident laser beam and surrounding points, yielding uncertainties typically within 2 GPa (see Additional file 1: Table S1 and Additional file 2: Table S2). Representative Raman spectra of the surface of the diamond anvils directly in contact with the sample and their differential spectra dI/dv (I intensity, v: wave number) from the different points are shown in Fig. 2. The high-frequency edge of the Raman band was defined as a minimum of dI/dv, which is determined by curve fitting using a Gaussian function. As shown in Fig. 2, we obtained very sharp peaks for the dI/dv function at each pressure point, even above 100 GPa. Brillouin spectra were collected at pressure conditions from 11 to 169 GPa in 1–13 GPa increments for SA1 and from 10 to 197 GPa in 2–15 GPa increments for SA2. The collecting time for each Brillouin scattering measurement was from 3 to 96 h. At each pressure, the raw Brillouin spectra of Stokes and anti-Stokes peaks were fitted with Lorentzian functions to obtain the peak positions.

Results and discussion

The RDFs showed that the first peaks observed in SA1 and SA2 were at 1.62 Å and at 1.65 Å, respectively (Fig. 1). As the Al-O bond length in the tetrahedral site is 0.13 Å longer than the Si-O bond length in the tetrahedral site (Shannon 1976), the average first nearest-neighbor T-O (T = Si, Al) lengths in SiO_2-Al_2O_3 glasses are longer than the Si-O length. These lengths for SA1 and SA2 were between that of SiO_2 glass (1.59 Å; Meade et al. 1992) and those of SiO_2 + 25.0 mol% Al_2O_3 glass

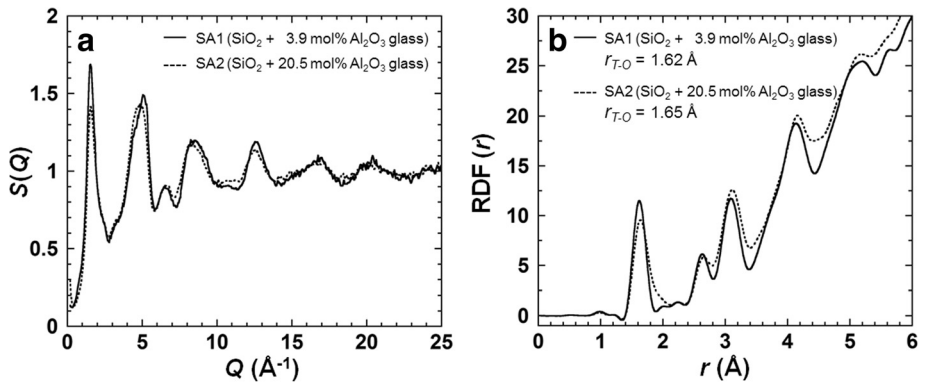

Fig. 1 **a** Total structure factors $S(Q)$ and **b** radial distribution functions of SA1 and SA2. The first neighbor T-O (T = Si, Al) lengths in SA1 and SA2 were 1.62 and 1.65 Å, respectively. The measurements were carried out in step-scanning mode with 0.05°/2θ in the range 0.3° < 2θ < 10.0°, 0.10°/2θ in the range 10.0° < 2θ < 19.9°, 0.15°/2θ in the range 19.9° < 2θ < 40.0°, and 0.20°/2θ in the range 40.0° < 2θ < 58.0° in transmission geometry. Incident X-ray energy was 61.55 keV and scattering vector (Q) changes were from 0.2 $Å^{-1}$ to 30.2 $Å^{-1}$

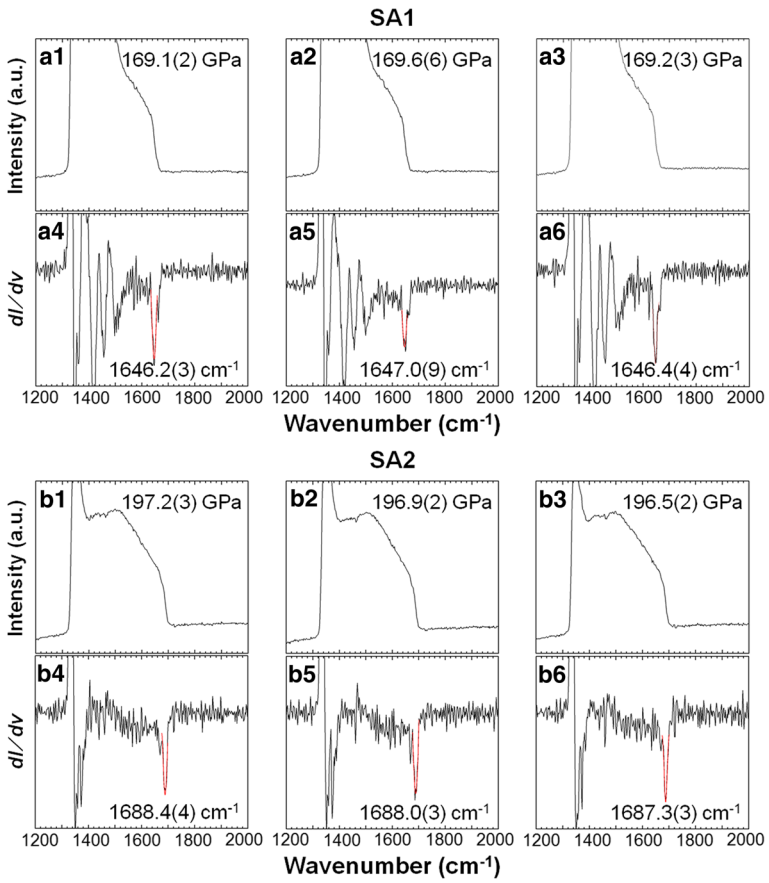

Fig. 2 Representative Raman spectra of different pressure conditions. Raman spectra were obtained from SA1 (SiO_2 + 3.9 mol% Al_2O_3) and SA2 (SiO_2 + 20.5 mol% Al_2O_3), respectively. They were measured from reflected light of the incident laser beam three times (*a1*, *a2*, *a3*, *b1*, *b2*, *b3*). Their differential spectra *dI / dv* are also shown (*a4*, *a5*, *a6*, *b4*, *b5*, *b6*). The high-frequency edge of the Raman band was defined as the minimum of the *dI / dv*. The *red lines* represent the fitting curves using Gaussian functions to determine the minimum position. *Numbers in parentheses* represent uncertainties in the last digit for both wave number and pressure. Uncertainties for the wave number of the minimum position of *dI / dv* in each spectrum were derived from the errors of the curve fitting. The total uncertainties for pressure were finally estimated from the standard deviation (1σ) of each determined pressure value at each point

(1.66 Å; Okuno et al. 2005) and SiO_2 + 28.2 mol% Al_2O_3 glass (1.75 Å; Morikawa et al. 1982), showing that our results were in agreement with previous studies about T-O lengths at ambient conditions.

Brillouin peaks from the transverse acoustic modes of both SA1 and SA2 were observed over the entire pressure range up to 169.3 and 196.9 GPa, respectively (Figs. 3, 4, and 5, Additional file 1: Table S1, Additional file 2: Table S2). The peaks from the longitudinal acoustic modes of those glasses were also observed at pressures below 45 GPa (a and b in Fig. 3). The peaks from the longitudinal acoustic modes were masked by those of the diamond transverse acoustic modes above 45 GPa (c and d in Fig. 3). As shown in Fig. 3, no significant peak broadening was observed with increasing pressure, indicating that the hydrostaticity in the sample chamber did not change significantly as the pressure changed (see also full width at half maximum (FWHM) in Additional file 1: Table S1 and Additional file 2: Table S2). The velocity uncertainties based on the difference between the peak positions of the Brillouin spectra of Stokes and anti-Stokes peaks were 0.8 % in SA1 and 0.3 % in SA2 on average throughout the pressure range measured (Additional file 1: Table S1 and Additional file 2: Table S2).

Variation in acoustic wave velocities with pressure was divided into three distinct pressure regions (Fig. 4): (i) the lowest pressure region where acoustic wave velocities increased rapidly up to 40 GPa; (ii) a high-pressure region from 40 to 100 GPa with a gentle gradient along a progressively flattening trend, and (iii) an ultrahigh-pressure region above 100 GPa, with an anomalously increasing V_S, which trend is highly consistent with that of previous works on SiO_2 and $MgSiO_3$ glasses (Murakami and Bass 2010, 2011).

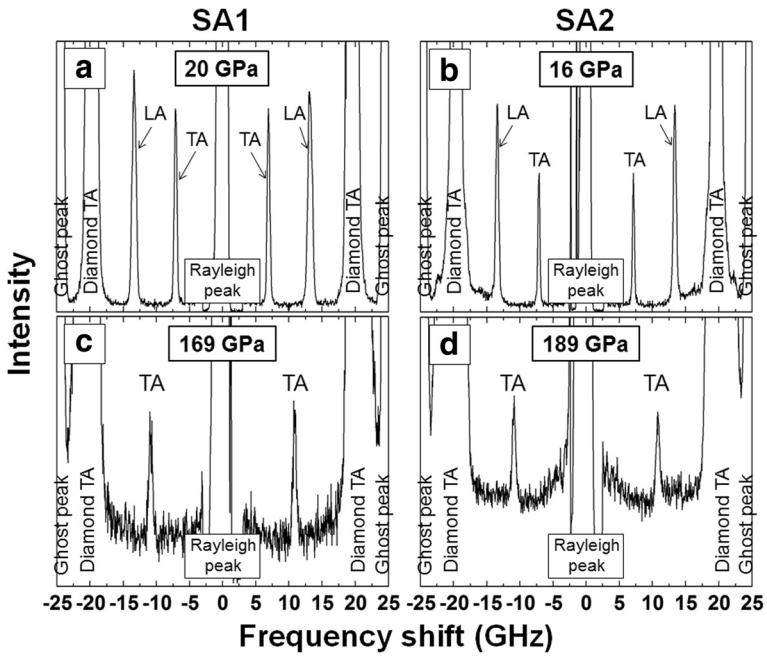

Fig. 3 In situ high-pressure Brillouin spectra. Spectra of **a** SA1 at 20 GPa, **b** SA2 at 16 GPa, **c** SA1 at 169 GPa, and **d** SA2 at 189 GPa. TA and LA indicate transverse and longitudinal acoustic modes of the Brillouin shift, respectively. Ghost peaks are artifacts of the interferometry method. LA peaks are masked above around 45 GPa because of the overlap of the diamond's TA peaks

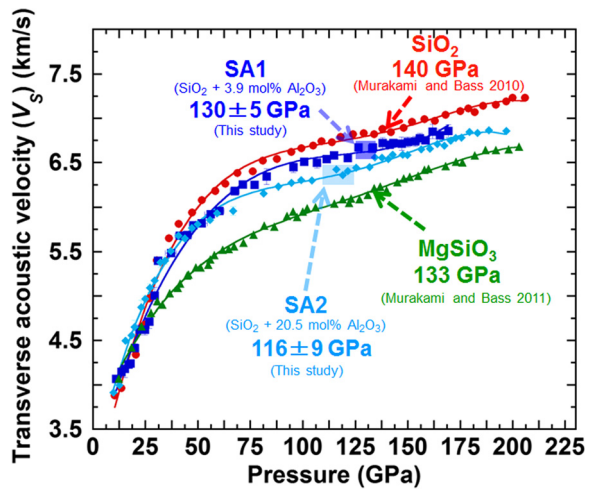

Fig. 4 *P-V_S* profiles up to 200 GPa. SA1 (*blue squares*, this study), SA2 (*light blue diamonds*, this study), SiO_2 glass (*red circles*, Murakami and Bass 2010), and $MgSiO_3$ glass (*green triangles*, Murakami and Bass 2011). The *curves* show the fourth order polynomial fitting of SA1 ($R^2 = 0.9960$), SA2 ($R^2 = 0.9978$), SiO_2 glass ($R^2 = 0.9964$), and $MgSiO_3$ glass ($R^2 = 0.9985$). The pressure conditions at which the increase of dV_S/dP occurs (the inflection pressure) are indicated by the *semi-transparent dark-blue box* (SA1) and the *semi-transparent light-blue box* (SA2)

Figure 5a shows the *P-V_S* profiles of SA1 and SA2 up to 40 GPa as functions of pressure together with those of SiO_2 glass (Murakami and Bass 2010) and $MgSiO_3$ glass (Murakami and Bass 2011). The values of V_S of the SiO_2-Al_2O_3 glasses increase rapidly from 10 to 40 GPa, with no discontinuous changes in slope. Figure 5b shows the regression curves of *P-V_S* plots of SA1 fitted to a fourth degree polynomial function and SA2 fitted to a quadratic function. The *P-V_S* profile of SA1 up to 40 GPa exhibited an increasing V_S with an inflection point at ~26 GPa. Such a trend was also observed in the *P-V_S* profile of SiO_2 glass (Murakami and Bass 2010). In contrast, the *P-V_S* profile of SA2 to 40 GPa can be fitted by a low-degree polynomial function such as a concave quadratic function (Fig. 5b), which is quite similar to that of $MgSiO_3$ glass (Murakami and Bass 2011). The *P-V_S* profile of SA2 below 40 GPa seems to be that of SA1 just shifted to lower pressures (Fig. 5). The difference in V_S in the pressure range from 10 to 40 GPa cannot be explained simply by density differences caused by the differing Al_2O_3 contents in SA1 and SA2. Previous studies on SiO_2-Al_2O_3 glasses at ambient conditions reported that the density of SiO_2-Al_2O_3 glasses increases with increasing Al_2O_3 content (Okuno et al. 2005). If we apply this density relationship in the SiO_2-Al_2O_3 system, the densities of SA1 and SA2 at ambient pressure can be estimated to be 2.24 and 2.40 g/cm^3, respectively, which are denser than pure SiO_2 glass (2.20 g/cm^3) (e.g., Brückner 1970). If the shear moduli for the two glasses

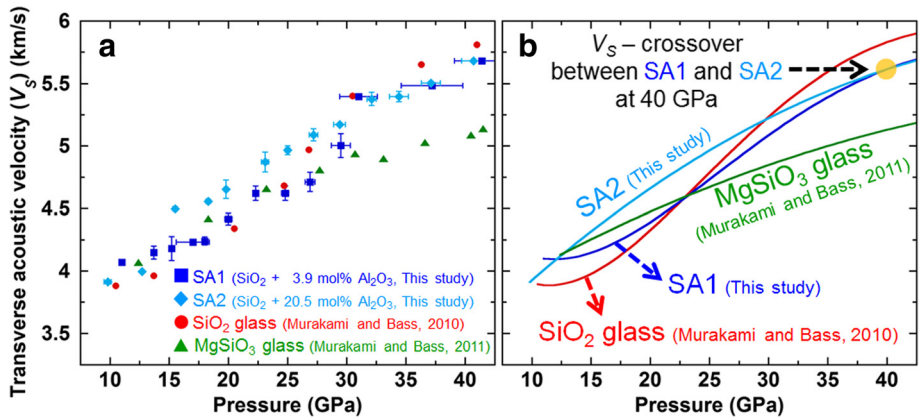

Fig. 5 Pressure-transverse acoustic wave velocity (*P*-V_S) profiles up to 40 GPa. **a** SA1 (*blue squares*, this study), SA2 (*light blue diamonds*, this study), SiO_2 glass (*red circles*, Murakami and Bass 2010), and $MgSiO_3$ glass (*green triangles*, Murakami and Bass 2011) up to 40 GPa. **b** Regression curves of SA1 and SA2 fitted by polynomial functions. *P*-V_S plots of SA1 from 11 to 60 GPa are fitted with a fourth order polynomial ($R^2 = 0.9933$) and *P*-V_S plots of SA2 from 10 to 59 GPa are fitted with a quadratic function ($R^2 = 0.9957$)

were equivalent, V_S would be expected to decrease as Al_2O_3 content increases in SiO_2-Al_2O_3 glasses because density is a term in the denominator in the formula of an acoustic wave velocity. However, the V_S of the "Al_2O_3-rich" SA2 is higher than that of the "Al_2O_3-poor" SA1 at pressures between 10 and 40 GPa. This *P*-V_S relation is thus likely to be due to differences in the elasticity/elastic moduli of SA1 and SA2, which appear in the numerator in the formula for acoustic wave velocity.

One possibility for explaining such an elasticity change is that the proportion of Al ions with large oxygen coordination numbers could depend on the Al_2O_3 content. A number of studies have shown that the average Al-O coordination numbers of aluminosilicate glasses always reach five and six at lower pressures than the average Si-O coordination number of SiO_2 glass and aluminosilicate glasses (e.g., Yarger et al. 1995; Lee et al. 2004; Allwardt et al. 2005; Drewitt et al. 2015; Benmore et al. 2010; Sato and Funamori 2010; Mysen and Richet 2005, and see also Additional file 3: Figure S1). In the present study, SA2 has more Al ion than SA1. In addition, some Al ions in SiO_2-Al_2O_3 glasses may be in 5- and 6-fold coordination with oxygen even at ambient pressure. This can serve as a network modifier, at least if the Al_2O_3 content is lower than 20.5 mol% (the composition of SA2). The Al ions in SA2 may be mainly in fourfold coordination with oxygen and serve as a network former, but about 40 % of the Al ions may exist in five- and sixfold coordination with oxygen at ambient pressure, as inferred from MD simulations for liquid SiO_2-Al_2O_3 (Poe et al. 1992a, b). Therefore, the proportion of Al ions with large oxygen coordination numbers (five- and sixfold Al) and the value of V_S in SA2 are always greater than in SA1 at isobaric conditions below 40 GPa. The increase of average Al-O coordination number of SA2 with increasing pressure may reflect its V_S increase. The V_S difference between SA1 and SA2 up to 40 GPa implies that aluminosilicate glasses become elastically stiffer as the proportion of five- and sixfold Al ion increases. In the present study, SA2 is elastically stiffer than SA1 at isobaric conditions between 10 and 40 GPa, and the *P*-V_S profile of SA2 seems, consequently, to be that of SA1 shifted to lower pressures.

The gradient of V_S with pressure becomes less steep above 40 GPa in contrast to its trend at lower pressures, which appears similar to the behavior of SiO_2 glass (Murakami and Bass 2010) and $MgSiO_3$ glass (Murakami and Bass 2011) (Fig. 4). Previous high-pressure experimental studies on SiO_2 glass showed that the Si-O coordination number of SiO_2 glass most likely changes from four to six up to ~40 GPa (Meade et al. 1992; Lin et al. 2007; Sato and Funamori 2008, 2010; Benmore et al. 2010; Zeidler et al. 2014) and that the sixfold coordination state may be preserved up to at least ~100 GPa (Sato and Funamori 2010). This behavior offers a reasonable explanation for the high-pressure acoustic wave velocity profile of SiO_2 glass (Murakami and Bass 2010). Because the trend of the *P*-V_S profile of SA1 is nearly identical to that of SiO_2 glass, SA1 also preserves the sixfold coordination state of Si, at least from 40 to 100 GPa. In contrast, the *P*-V_S profile of SA2 is convex upward with a gentle gradient from 10 to around 100 GPa, which is similar to that observed in $MgSiO_3$ glass (Murakami and Bass 2011). This gradually increasing V_S for SA2, similar to that of $MgSiO_3$ glass up to at least 100 GPa, also suggests that the average Si-O coordination number increases gradually from four to six in this pressure region.

The values of V_S for SA1 and SA2 increase more rapidly as pressure grows past ~100 GPa (Fig. 4), which was

also observed in SiO_2 glass (Murakami and Bass 2010) and $MgSiO_3$ glass (Murakami and Bass 2011). Such dV_S/dP changes observed above ~100 GPa have previously been interpreted to reflect the onset of the average Si-O coordination number changing from just 6 to 6^+ (Murakami and Bass 2010, 2011). This conclusion subsequently found support in the results from MD computer simulations (Brazhkin et al. 2011; Wu et al. 2012). To determine the pressure conditions at which this abrupt change of dV_S/dP occurs, we adopted the same criteria as Murakami and Bass (2010, 2011). Each P-V_S profile was fitted to fourth and fifth polynomial functions of pressure with an adjusted R-square of above 0.995. The pressure conditions at the onset of the rapid V_S increase in the P-V_S profiles of SA1 and SA2 were determined by calculating the point at which the second derivative of the fitted polynomial functions with respect to pressure (d^2V_S/dP^2) is a maximum. The pressure conditions at which the increase of dV_S/dP occur (hereafter referred to as "the inflection pressure") are 130 ± 5 GPa in SA1 and 116 ± 9 GPa in SA2. The inflection pressure of SA1 is 10 GPa lower than that of SiO_2 glass (Murakami and Bass 2010) and 3 GPa lower than that of $MgSiO_3$ glass (Murakami and Bass 2011). The inflection pressure of SA2 is 24 GPa lower than that of SiO_2 glass (Murakami and Bass 2010) and 17 GPa lower than that of $MgSiO_3$ glass (Murakami and Bass 2011).

Such a change of dV_S/dP may indicate the onset of further structural change in silicate glasses resulting from an average Si-O coordination number increase from 6 to 6^+. Our results may suggest that the inflection pressure does not strongly depend on the amount of metal ions because the M/Si (M = Mg, Al) values for SA1 and SA2 are less than for $MgSiO_3$ glass, which has much higher inflection pressure than SA1 and SA2 (Fig. 6). This indicates that Al_2O_3 is much more effective than MgO in reducing the pressure at which the average Si-O coordination number starts to increase from 6 to 6^+. Another explanation of the lowered inflection pressure is that the average Al-O coordination numbers increase from 6 to 6^+ at a lower pressure than do those of Si-O, similar to the transition of average Al-O coordination number from 4 to 6 that occurs at lower pressures than the transition of Si-O. However, no study has yet indicated the different pressures at which the average Al-O and Si-O coordination numbers exceed 6. In addition, the P-V_S profiles of SA1 and SA2 have only one inflection point, at the onset of the average Si-O coordination number's increase from 6 to 6^+ (Brazhkin et al. 2011; Wu et al. 2012; Murakami and Bass 2010, 2011). Therefore, the inflection points under ultrahigh pressure may primarily reflect a change of the average Si-O coordination number from 6 to 6^+.

Density increases caused by structural transitions accompanied by Si-O coordination number growth occur continuously in glasses and melts and occur discontinuously in crystalline materials (e.g., Loerting et al. 2009). Although it is not obvious whether the analogy between silicate glasses and silicate melts works well as a model of their structural or density changes with pressure, experimental results on the evolution of average Si-O coordination number of SiO_2 glass (Meade et al. 1992; Lin et al. 2007; Sato and Funamori 2008, 2010; Benmore et al. 2010; Zeidler et al. 2014) shows good agreement with that of SiO_2 melt calculated by MD simulations (Karki et al. 2007). A recent experimental study

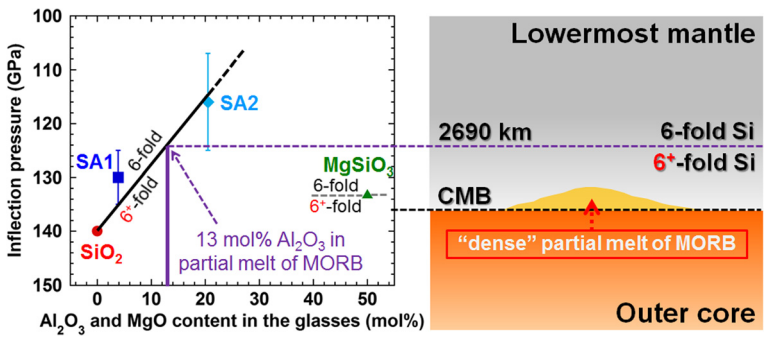

Fig. 6 Inflection pressures in the P-V_S profiles of the silicate glasses. SA1 (*blue square*, this study), SA2 (*light blue diamond*, this study), SiO_2 glass (*red circle*, Murakami and Bass 2010), and $MgSiO_3$ glass (*green triangle*, Murakami and Bass 2011) are shown in the *left graph*. This is regarded as the onset of the average Si-O coordination number increasing from 6 to 6^+ ("*6^+-fold (Si)*" in this figure) in each glass (see Murakami and Bass 2010, 2011). The *solid black line* shows the possible transitional boundary at which the average Si-O coordination number increases from 6 to 6^+ in SiO_2-Al_2O_3 glasses, calculated using a linear leasts squares method based on the plots of SiO_2 glass, SA1, and SA2. The pressure-intercept is fixed at 140 GPa, derived from the inflection pressure of SiO_2 glass reported by Murakami and Bass (2010). Assuming an Al_2O_3 content of 13 mol% in an SiO_2-Al_2O_3 glass, the average Si-O coordination number is expected to exceed 6 at 124 GPa (*purple lines*), which corresponds to a depth of 2690 km, much shallower than the CMB. The *dashed gray line* shows the boundary at which the average Si-O coordination number increases from just 6 to 6^+ in $MgSiO_3$ glass. The picture on the right is a schematic image of the accumulation of "dense" partial melts having structures governed by 6^+-fold Si, generated from MORBs

suggested that the Si-O coordination state in molten basalt is roughly consistent with that in SiO_2 glass and melt up to 60 GPa (Sanloup et al. 2013). If this is the case, the pressure-induced acoustic wave velocity changes of the aluminosilicate glasses explored in the present study may offer possible implications for the dynamics of dense magmas that potentially exist at the base of the mantle. The possible existence of dense silicate melts at or near the CMB has been proposed (e.g., Ohtani 1983; Ohtani and Maeda 2001; Williams and Garnero 1996; Labrosse et al. 2007) to explain the anomalous reduction of the seismic wave velocities just above the CMB (e.g., Garnero and Helmberger 1995; Mori and Helmberger 1995). Recent high-pressure melting experiments indicated that such dense silicate melts at the CMB can be generated by partial melting of mid-ocean ridge basalts (MORBs) (Andrault et al. 2014; Pradhan et al. 2015). The densification in SA1 and SA2, which probably reflects an average Si-O coordination number in excess of 6, occurs at lower pressures than in pure $MgSiO_3$ glass (Fig. 6). Figure 6 shows the inflection pressure as a function of Al_2O_3 contents in the SiO_2-Al_2O_3 system, indicating a linear relationship. If we assume that an Al_2O_3 content of ~13 mol% may possibly be included in partial melts of MORBs generated at around 100 GPa (Pradhan et al. 2015), the inflection pressure is expected to be 124 GPa corresponding to a depth of ~2690 km. The silicate melts generated by the partial melting of MORBs might thus undergo a structural transformation involving possible densification changes related to Si-O coordination states at depths of around ~2690 km, which is clearly shallower than the CMB.

Although the possibility of densification processes in the silicate melts occurring due to the addition of heavy elements such as Fe cannot be ruled out, the increases in density associated with structural changes in Si-O coordination states that possibly take place at pressures within the lower mantle might also play an important role in the dynamics of silicate melts at the base of the mantle.

Conclusions

The transverse acoustic wave velocities of SiO_2-Al_2O_3 glasses were measured at pressures up to near 200 GPa. At pressures from 10 to 40 GPa, the V_S of the Al_2O_3-rich SA2 is higher than that of the Al_2O_3-poor SA1, which is likely related to differences in the elasticity/elastic moduli between SA1 and SA2. Such a difference in the elasticity may be derived from the different proportions of five- and sixfold Al ions in those glasses. The dV_S/dP gradients of both SA1 and SA2 became less steep at pressures from 40 to 100 GPa. In this pressure range, SA1 had a P-V_S profile nearly identical to that of SiO_2 glass, indicating that the sixfold coordinated structure is preserved. SA2, however, had a P-V_S profile similar to that of $MgSiO_3$ glass, suggesting a gradually increasing average Si-O coordination number from 4 to 6 up to around 100 GPa. dV_S/dP also increases at 130 ± 5 GPa in SA1 and at 116 ± 9 GPa in SA2, which can be interpreted as the onset of the average Si-O coordination number change from 6 to 6^+. The inflection pressures for SA1 and SA2 are much lower than in $MgSiO_3$ glass, suggesting that Al_2O_3 promotes the reduction of pressure conditions of inflection caused by an increase of the average Si-O coordination number from 6 to 6^+ much more strongly than does MgO. Such a densification mechanism associated with the Si-O coordination number change may play a key role in the gravitational stabilization of the partial melting of MORBs within the lowermost mantle deeper than 2690 km.

Additional files

Additional file 1: Table S1. Data of Raman and Brillouin scattering spectra for SA1. Peak position of the Raman differential spectrum (*dI / dv*) for pressure determination (*R* peak), pressure (*P*) and transverse acoustic wave velocity (V_S) of SA1 (SiO_2 + 3.9 mol% Al_2O_3), and full width at half maximum (FWHM) of the Brillouin peak from TA mode. (PDF 125 kb)

Additional file 2: Table S2. Data of Raman and Brillouin scattering spectra for SA2. Peak position of the Raman differential spectrum (*dI / dv*) for pressure determination (*R* peak), pressure (*P*) and transverse acoustic wave velocity (V_S) of SA2 (SiO_2 + 3.9 mol% Al_2O_3), and full width at half maximum (FWHM) of the Brillouin peak from TA mode. (PDF 129 kb)

Additional file 3: Figure S1. Summary of the pressure dependence of average coordination numbers (CNs) of Al-O in aluminosilicate glasses and average CNs of Si-O in SiO_2 glass. The results of aluminosilicate glasses from NMR spectroscopy and in situ XRD results are indicated by red symbols. Pressure-recovered glasses are used for NMR studies. The in situ XRD results of pure SiO_2 are also indicated by open symbols. Details of references are as follows: Ab50NTS50 (red square, Y95) shows data for $(NaAlSi_3O_8)_{0.5}(Na_2Si_4O_9)_{0.5}$ glass using NMR spectroscopy by Yarger et al. (1995); NAS150560 (red circle, L04) and NAS6 (red diamond, L04) show data for $(Na_2O)_{0.75}(Al_2O_3)_{0.25}3SiO_2$ glass and $NaAlSi_3O_8$ glass using NMR spectroscopy by Lee et al. (2004); KAS (red triangle, A05), NAS (red inversed triangle, A05), and CAS (red pentagon, A05) show data for $K_3AlSi_3O_9$ glass, $Na_3AlSi_3O_9$ glass, and $Ca_3Al_2Si_6O_{18}$ glass using NMR spectroscopy by Allwardt et al. (2005). An glass (red star, D15) shows data for $CaAl_2Si_2O_8$ glass using in situ XRD results by Drewitt et al. (2015); SiO_2 glass (blue square, B10) shows data for pure SiO_2 glass using in situ XRD by Benmore et al. (2010); SiO_2 glass (blue circle, S10) shows data for pure SiO_2 glass using in situ XRD by Sato and Funamori (2010). (TIF 221 kb)

Abbreviations

CMB, core-mantle boundary; MD, molecular dynamics; MORBs, mid-ocean ridge basalts; NMR, nuclear magnetic resonance; RDF, radial distribution function; SA1, SiO_2 + 3.9 mol% Al_2O_3 glass; SA2, SiO_2 + 20.5 mol% Al_2O_3 glass; SEM-EDS, scanning electron microscope with energy-dispersive X-ray spectrometer; ULVZs, ultralow velocity zones; V_P, longitudinal acoustic wave velocity; V_S, transverse acoustic wave velocity.

Competing interests

The authors declare that they have no competing interests.

Authors' contributions

IO and MM performed the Brillouin scattering measurements. IO, MM, SK, and KO synthesized and analyzed the glassy starting materials. IO, MM, and KO wrote the paper. All authors discussed the results and commented on the manuscript. All authors read and approved the final manuscript.

Acknowledgements
The authors thank T. Sakamaki for his useful discussions. The authors also thank T. Nishimoto for his technical support on the Brillouin scattering measurements. This work was supported by JSPS KAKENHI grant numbers 22684028 and 21654075 awarded to MM and 15H05748 awarded to EO. The synchrotron radiation experiments were performed at the BL04B2 unit of the SPring-8 facility with the approval of the Japan Synchrotron Radiation Research Institute (JASRI) (proposal no. 2011B1159).

Author details
[1]Department of Earth Science, Graduate School of Science, Tohoku University, Sendai 980-8578, Japan. [2]Research and Utilization Division, Japan Synchrotron Radiation Research Institute, Sayo, Hyogo 679-5198, Japan. [3]Present address: Synchrotron X-ray Group, Quantum Beam Unit, Advanced Key Technologies Division, National Institute for Materials Science (NIMS), Sayo, Hyogo 679-5148, Japan. [4]V.S. Sobolev Institute of Geology and Mineralogy, Siberian Branch, Russian Academy of Sciences, Novosibirsk 630090, Russia.

Received: 6 January 2016 Accepted: 14 June 2016
Published online: 29 June 2016

References

Akahama Y, Kawamura H (2004) High-pressure Raman spectroscopy of diamond anvils to 250 GPa: method for pressure determination in the multimegabar pressure range. J Appl Phys 96:3748–3751
Allwardt JR, Stebbins JF, Schmidt BC, Frost DJ, Withers AC, Hirschmann MM (2005) Aluminum coordination and the densification cation of high-pressure aluminosilicate glasses. Am Mineral 90:1218–1222
Allwardt JR, Stebbins JF, Terasaki H, Du L-S, Frost DJ, Withers AC, Hirschmann MM, Suzuki A, Ohtani E (2007) Effect of structural transitions on properties of high-pressure silicate melts: ^{27}Al NMR, glass densities, and melt viscosities. Am Mineral 92:1093–1104
Andrault D, Pesce G, Bouhifd MA, Bolfan-Casanova N, Hénot J-M, Mezouar M (2014) Melting of subducted basalt at the core-mantle boundary. Science 344:892–985
Benmore CJ, Soignard E, Amin SA, Guthrie M, Shastri SD, Lee PL, Yarger JL (2010) Structural and topological changes in silica glass at pressure. Phys Rev B 81: 054105
Brazhkin VV, Lyapin AG, Trachenko K (2011) Atomistic modeling of multiple amorphous- amorphous transitions in SiO_2 and GeO_2 glasses at megabar pressures. Phys Rev B 83:132103
Brückner R (1970) Properties and structure of vitreous silica I. J Non-Cryst Solids 5: 123–175
Drewitt JWE, Jahn S, Sanloup C, Grouchy C, Garbarino G, Hennet L (2015) Development of chemical and topological structure in aluminosilicate liquids and glasses at high pressure. J Phys Condens Matter 27:105103
Garnero EJ, Helmberger DV (1995) A very slow basal layer underlying large-scale low-velocity anomalies in the lower mantle beneath the Pacific: evidence from core phases. Phys Earth Planet Inter 91:161–176
Garnero EJ, Revenaugh J, Williams Q, Lay T, Kellogg LH (1998) Ultralow velocity zone at the core-mantle boundary. In: Gurnis M, Wysession ME, Knittle E, Buffett BA (eds) The core-mantle boundary region, vol 28, Geodynamics series. AGU, Washington DC, pp 319–334
Karki BB, Bhattarai D, Stixrude L (2007) First-principles simulations of liquid silica: structural and dynamical behavior at high pressure. Phys Rev B 76:104205
Kato D (1976) Raman spectrum and refractive index behavior of Al_2O_3-added high-silica-content glass. J Appl Phys 47:5344–5348
Kohara S, Itou M, Suzuya K, Inamura Y, Sakurai Y, Ohishi Y, Takata M (2007) Structural studies of disordered materials using high-energy x-ray diffraction from ambient to extreme conditions. J Phys Condens Matter 19:506101
Labrosse S, Hernlund JW, Coltice N (2007) A Crystallizing dense magma ocean at the base of the Earth's mantle. Nature 450:866–869
Lee SK, Cody GD, Fei Y, Mysen BO (2004) Nature of polymerization and properties of silicate melts and glasses at high pressure. Geochim Cosmochim Acta 68:4189–4200
Lin J-F, Fukui H, Prendergast D, Okuchi T, Cai YQ, Hiraoka N, Yoo C-S, Trave A, Eng P, Hu MY, Chow P (2007) Electronic bonding transition in compressed SiO_2 glass. Phys Rev B 75:012201
Linh NN, Hoang VV (2007) Structural properties of simulated liquid and amorphous aluminium silicates. Phys Scr 76:165–172
Loerting T, Brazhkin VV, Morishita T (2009) Multiple amorphous-amorphous transitions. Adv Chem Phys 143:29–82
Mashino I, Murakami M, Ohtani E (2016) Sound velocities of δ-AlOOH up to core-mantle boundary pressures with implications for the seismic anomalies in the deep mantle. J Geophys Res 121:595–609
McMillan P, Piriou B (1982) The structures and vibrational spectra of crystals and glasses in the silica-alumina system. J Non-Cryst Solids 53:279–298
Meade C, Hemley RJ, Mao H-K (1992) High-pressure X-ray diffraction of SiO_2 glass. Phys Rev Lett 69:1387–1390
Mori J, Helmberger DV (1995) Localized boundary layer below the mid-Pacific velocity anomaly identified from a PcP precursor. J Geophys Res 100:20359–20365
Morikawa H, Miwa S, Miyake M, Marumo F, Sata T (1982) Structural analysis of SiO_2-Al_2O_3 glasses. J Am Ceram Soc 65:78–81
Murakami M, Bass JD (2010) Spectroscopic evidence for ultrahigh-pressure polymorphism in SiO_2 glass. Phys Rev Lett 104:025504
Murakami M, Bass JD (2011) Evidence of denser $MgSiO_3$ glass above 133 gigapascal (GPa) and implications for remnants of ultradense silicate melt from a deep magma ocean. Proc Natl Acad Sci U S A 108:17286–17289
Mysen BO, Richet P (2005) Silicate glasses and melts: properties and structure. Developments in geochemistry. Elsevier, New York
Ohtani E (1983) Melting temperature distribution and fractionation in the lower mantle. Phys Earth Planet Inter 33:12–25
Ohtani E, Maeda M (2001) Density of basaltic melt at high pressure and stability of the melt at the base of the lower mantle. Earth Planet Sci Lett 193:69–75
Okuno M, Zotov N, Schmücker M, Schneider H (2005) Structure of SiO_2-Al_2O_3 glasses: combined X-ray diffraction, IR and Raman studies. J Non-Cryst Solids 351:1032–1038
Petitgirard S, Malfait WJ, Sinmyo R, Kupenko I, Hennet L, Harries D, Dane T, Burghammer M, Rubie DC (2015) Fate of $MgSiO_3$ melts at core-mantle boundary conditions. Proc Natl Acad Sci U S A 112:14186–14190
Poe BT, McMillan PF, Angell CA, Sato RK (1992a) Al and Si coordination in SiO_2-Al_2O_3 glasses and liquids: a study by NMR and IR spectroscopy and MD simulations. Chem Geol 96:333–349
Poe BT, McMillan PF, Coté B, Massiot D, Coutures J-P (1992b) SiO_2-Al_2O_3 liquids: in-situ study by high-temperature ^{27}Al NMR spectroscopy and molecular dynamics simulation. J Phys Chem 96:8220–8224
Pradhan GK, Fiquet G, Siebert J, Auzende A-L, Morard G, Antonangeli D, Garbarino G (2015) Melting of MORB at core–mantle boundary. Earth Planet Sci Lett 431:247–255
Risbud SH, Kirkpatrick RJ, Taglialavore AP, Montez B (1987) Solid-state NMR evidence of 4-, 5-, and 6-fold aluminum sites in roller-quenched SiO_2-Al_2O_3 glasses. J Am Ceram Soc 70:C10–C12
Sanloup C, Drewitt JWE, Konôpková Z, Dalladay-Simpson P, Morton DM, Rai N, van Westrenen W, Morgenroth W (2013) Structural change in molten basalt at deep mantle conditions. Nature 503:104–107
Sato T, Funamori N (2008) Sixfold-coordinated amorphous polymorph of SiO_2 under high pressure. Phys Rev Lett 101:255502
Sato T, Funamori N (2010) High-pressure structural transformation of SiO_2 glass up to 100 GPa. Phys Rev B 82:184102
Sato RK, McMillan PF, Dennison P, Dupree R (1991) High-resolution ^{27}Al and ^{29}Si MAS NMR investigation of SiO_2-Al_2O_3 glasses. J Phys Chem 95:4483–4489
Sen S, Youngman RE (2004) High-resolution multinuclear NMR structural study of binary aluminosilicate and other related glasses. J Phys Chem B 108:7557–7564
Shannon RD (1976) Revised effective ionic radii and systematic studies of interatomic distances in halides and chalcogenides. Acta Crystallogr Sect A 32:751–767
Weber R, Sen S, Randall E, Youngman RE, Hart RT, Benmore CJ (2008) Structure of high alumina content Al_2O_3-SiO_2 composition glasses. J Phys Chem B 112: 16726–16733
Whitfield CH, Brody EM, Bassett WA (1976) Elastic moduli of NaCl by Brillouin scattering at high pressure in a diamond anvil cell. Rev Sci Instrum 47:942–947
Williams Q, Garnero EJ (1996) Seismic evidence for partial melt at the base of Earth's mantle. Science 273:1528–1530
Wu M, Liang Y, Jiang J-Z, Tse JS (2012) Structure and properties of dense silica glass. Scientific Reports 2:398
Yarger JL, Smith KH, Nieman RA, Diefenbacher J, Wolf GH, Poe BT, McMillan PF (1995) Al coordination changes in high-pressure aluminosilicate liquids. Science 270:1964–1967

Zeidler A, Wezka K, Rowlands RF, Whittaker DAJ, Salmon PS, Polidori A, Drewitt JWE, Klotz S, Fischer HE, Wilding MC, Bull CL, Tucker MG, Wilson M (2014) High-pressure transformation of SiO_2 glass from a tetrahedral to an octahedral network: a joint approach using neutron diffraction and molecular dynamics. Phys Rev Lett 113:135501